Monitoring the Early Steps of Unfolding of Dicalcium and Mono-Ce 3+-Substituted Forms of P43M Calbindin D9k

ARTICLE *in* BIOCHEMISTRY · DECEMBER 2003

Impact Factor: 3.02 · DOI: 10.1021/bi034638+ · Source: PubMed

3 AUTHORS, INCLUDING:

Beatriz Jiménez
Imperial College London
29 PUBLICATIONS **465** CITATIONS
SEE PROFILE

Mario Piccioli
University of Florence
99 PUBLICATIONS **2,315** CITATIONS
SEE PROFILE

Monitoring the Early Steps of Unfolding of Dicalcium and Mono-Ce^{3+}-Substituted Forms of P43M Calbindin D_{9k}[†]

Beatriz Jiménez,[‡] Luisa Poggi,[§] and Mario Piccioli*[,§]

Departamento de Química Inorgánica, University of Valencia, Dr. Moliner, 50, 46100 Burjasot, Valencia, Spain, and Magnetic Resonance Center (CERM), University of Florence, Via L. Sacconi 6, 50019 Sesto Fiorentino, Florence, Italy

Received April 22, 2003; Revised Manuscript Received August 27, 2003

ABSTRACT: Early steps of unfolding of P43M Calbindin D_{9k} have been evaluated by NMR spectroscopy on the native dicalcium and on the paramagnetic monocerium-substituted derivative. Although at 2 M GdmHCl the protein core maintains its overall folding and structure, amide ^{15}N R_2 measurements and cross correlation rates between N−H dipole−dipole relaxation and ^{15}N CSA relaxation reveal a closer and stronger packing of the hydrophobic interactions in the protein as a response to the presence of denaturing agents in solution. A complete reorientation of the Met43 side chain toward the hydrophobic core is accomplished by the disappearance of the millisecond dynamics observed on the native form of Calbindin D_{9k}, while cross correlation rates provide evidence that the two-way hydrogen bond between Leu23 and Val61 is broken or substantially weakened. The substitution of the calcium ion in site II with the paramagnetic Ce^{3+} ion allowed us to obtain a number of long-range nonconventional constraints, namely, pseudocontact shifts, which were used, together with the NOEs collected on the native state, to monitor subtle structural variations occurring in the non-native state of the protein. Although the average rmsd between the structures of native and non-native states is small (0.48 Å), structural rearrangements could be reliably identified. Our results provide unprecedented information about the behavior of Calbindin D_{9k} during the early steps of unfolding. Furthermore, they constitute strong evidence of the efficiency of paramagnetism-based constraints in monitoring subtle structural changes that are beyond the sensitivity of an approach based only on NOE.

Calcium ion is an important second messenger in a wide variety of cellular functions (*1*). As a consequence, calcium binding proteins make up an abundant and well-studied class of metalloproteins. One group of such proteins is characterized by a helix−loop−helix structure known as an EF-hand (*2*). Often, two or more EF-hand motifs are connected via a flexible linker segment that may lead to cooperative interactions between the Ca^{2+} binding centers. A particularly well studied example of an EF-hand is the small (8.5 kDa) calcium binding protein Calbindin D_{9k}. Calbindin D_{9k} (Cb hereafter) is a dicalcium binding protein consisting of four helices and two EF-hands joined together by a flexible linker region with one metal ion bound to each of the two loops. The calcium binding ligands are arrayed around the loops in the EF-hand motif and coordinate the calcium ion with a similar geometry but with different topology of the two loops (*2*). In the second site (classical EF-hand), most of the ligands are contributed from carboxyl ligands of aspartic and glutamic side chains, with the last being a bidentate Glu ligand. The first site contains a two-residue insertion which leads to an alternation of the loop conformation. This causes the calcium ion to be coordinated by the backbone carbonyls instead of the side chain carbonyls, with the exception of the bidentate Glu that is still present. Site I is therefore termed a "pseudo-EF-hand" (*2*).

The coordination differences between the two metal binding sites of Cb allow the selective substitution of the calcium ion in site II with a lanthanide (*3*). Lanthanide ions have long been used as probes for the spectroscopically silent Ca^{2+} ion in many calcium ion binding proteins (*4*−*6*). Structures of the apo, dicalcium (Ca_2Cb), and lanthanide-substituted (CaLnCb) complexes have all been determined by either NMR[1] or X-ray diffraction techniques (*7*−*9*). Magnetic properties of lanthanide ions have been used to obtain information about the structure and function of the native Ca^{2+} systems. There is structural and spectroscopic

[†] This work was supported by European Union Research and Training Network (RTN) Project "Cross correlation between the fluctuations of different interactions: a new avenue for biomolecular NMR" (Contract HPRN-CT-2000-00092) and by RTD Project "Transient NMR" (Contract HPRI-CT-1999−5006). The work has been performed at the EU Large Scale Facility PARABIO (Contract HPRI-CT-1999−00009). B.J. is a fellow of the Marie Curie Training Site NMR in Inorganic Structural Biology (Contract HPMT-2000-000137). B.J. thanks the Generalitat Valenciana for a Ph.D. grant.

* To whom correspondence should be addressed: Magnetic Resonance Center (CERM), University of Florence, Via L. Sacconi 6, 50019 Sesto Fiorentino, Florence, Italy. Fax: +39 055 457 4253. Phone: +39 055 457 465. E-mail: piccioli@cerm.unifi.it.

[‡] University of Valencia.

[§] University of Florence.

[1] Abbreviations: NMR, nuclear magnetic resonance; CSA, chemical shift anisotropy; HSQC, heteronuclear single-quantum correlation; FHSQC, fast heteronuclear single-quantum correlation; CLEANEX-PM, phase-modulated clean chemical exchange; NOE, nuclear Overhauser effect; WT, wild type; P43G, Calbindin D_{9k} mutant with a Pro43 → Gly substitution; P43M, Calbindin D_{9k} mutant with a Pro43 → Met substitution. Amino acids are denoted by their standard one- and three-letter codes.

10.1021/bi034638+ CCC: $25.00
Published on Web 10/17/2003

evidence that, despite the differences in charge between the lanthanide and calcium ions, replacement of the latter causes only very minor structural rearrangements (*10*), thus justifying the use of lanthanides as structural probes.

The four-helix bundle domain is a commonly occurring fold in which the amphipathic helices pack against one another to form a hydrophobic core of nonpolar residues from all four helices. The polar residues on the outer sides of the helices decorate the surface of the domain and solubilize it. The four-helix bundle fold allows extensive changes in tertiary packing to occur without a significant change in the secondary structure. Calbindin D_{9k} is supposed to bind calcium after folding, and the metal is known to stabilize the protein (*11*). Cb has no sulfide bonds and a high surface charge density that leads to significant destabilizing charge−charge repulsion (*12*) in the apo form. However, the protein is extremely stable ($T_m \sim 85$ °C) (*13*), pointing to important contributions to the stability from the core residues that more than compensate for the electrostatic repulsions. It has also been reported that the two subdomains produced by cleavage of the linker loop between the two EF-hands form heterodimers when mixed in the presence of Ca^{2+} and reconstitute the intact structure (*14*).

In its Ca^{2+}-bound state, the protein is resistant to thermal denaturation and stays folded in 10 M urea (*11*). We expect that the presence of denaturing agents induces changes to both protein structure and protein dynamics even at concentrations much lower than those in which a decrease in secondary structure content is observed. Even if there is no biological relevance to a partially destabilized Calbindin, such subtle changes should be carefully investigated because they are likely to point out protein regions that are affected by denaturing agents and to identify intramolecular interactions providing the driving force that initiates the folding process.

The structural characterization of proteins under non-native conditions is a key step in understanding relationships between protein folds and protein functions. It can provide valuable insights into several issues of modern biophysics (*15*−*17*). NMR spectroscopy is one of the most useful techniques applied for structural characterization of denatured or partially unfolded states (*18*−*27*). Both kinetic and thermodynamic aspects of unfolding and refolding processes can be addressed at the atomic level. In this work, we have been interested in studying the effect of the denaturant guanidinium chloride (GdmHCl) on the structural and dynamic properties of the dicalcium, mono-Ce^{3+}-substituted, and apo forms of Calbindin D_{9k}. We will assess how paramagnetic probes may contribute to the structural characterization of unfolded states, providing reliable long-range distance restraints.

MATERIALS AND METHODS

Sample Preparation

Protein expression (*28*) and purification (*29*) of both the Ca^{2+} and apo forms of the bovine Pro43 → Met (P43M) mutant (*30*, *31*) of Calbindin D_{9k} were performed as reported. The P43M mutation eliminates the conformational heterogeneity due to cis−trans isomerism of this proline residue (*31*). The expression system was a generous gift of S. Forsén. Uniformly ^{15}N-labeled overexpressed P43M was obtained from M9 minimal medium containing $(^{15}NH_4)_2SO_4$ as the sole nitrogen source. The site II cerium substitution procedure is described elsewhere (*3*). Apo-Cb was obtained by washing the dicalcium sample with a 0.5 mM solution of DOTA (1,4,7,10-tetraazacyclododecane-1,4,7,10-tetraacetic acid). The pH was adjusted to 6.0 with 0.1 M NaOH or 0.1 M HCl. The final concentration of all samples was approximately 1.0 mM with a sample volume of 305 μL (10% D_2O/90% H_2O). A 7 M GdmHCl aqueous solution was prepared and its pH adjusted to 6.0 by adding small quantities of NaOH or HCl. Aliquots of this GdmHCl solution were added to NMR samples in successive steps in which the following concentrations of denaturant were achieved: 0.20, 0.41, 0.79, 1.21, 1.65, and 2.08 M. The samples were kept at 4 °C between measurements.

NMR Experiments

All NMR experiments were carried out at 300 K on Bruker Avance 400 and 700 spectrometers.

Nonlabeled Ca_2Cb and CaCeCb Samples. One-dimensional (1D) NMR experiments using a spectral width of 16 ppm and a recycle time of 1 s were performed after each addition of GdmHCl at 16.4 T (700 MHz proton Larmor frequency). To investigate the region of hyperfine-shifted signals, experiments were also carried out over a 60 ppm spectral width using a recycle delay of 200 ms.

^{15}N-Labeled Ca_2Cb Sample. Two-dimensional (2D) ^1H−^{15}N HSQC experiments were performed at 16.4 T (700 MHz proton Larmor frequency) after each addition of GdmHCl. Spectra were acquired using 128 × 2048 complex points and spectral widths of 30.0 and 16.0 ppm in the t_1 and t_2 dimensions, respectively. The ^1H carrier frequency was set coincident with the water resonance; the ^{15}N carrier frequency was set to 116.0 ppm. The recycle delay was 1 s. A total of four transients were recorded for each complex point. The free induction decays were processed in F_2 by apodizing with a cosine bell window function, zero-filling once, and Fourier-transforming. The resulting spectra were phased and baseline-corrected. The F_1 interferograms were apodized with a cosine bell window function, zero-filled once, Fourier-transformed, and phase-corrected.

^{15}N $R_2(1/\tau_{cp})$ relaxation rates at 9.4 T (400 MHz proton Larmor frequency) were measured using the relaxation-compensated Carr−Purcell−Meiboom−Gill (CPMG) pulse sequences previously reported in the literature (*32*) on the sample containing 2 M GdmHCl. Data were collected for τ_{cp} values of 1.0, 1.5, 2.0, 4.0, 6.6, 10.8, 21.5, and 64.5 ms. Acquisition conditions were the same as those for the ^1H−^{15}N HSQC experiment.

Cross correlation between ^{15}N−^1H dipolar interaction and ^{15}N CSA measurements were carried out at 16.4 T (700 MHz proton Larmor frequency) using a previously reported sequence (*33*) on the sample containing 2 M GdmHCl. Durations for the dephasing delay, during which the buildup of cross correlation takes place, were 46.7, 68, and 132 ms. Fast amide proton exchange rates were measured on the 2 M GdmHCl sample using ^{15}N (CLEANEX-PM)−FSQC experiments (*34*, *35*) with a mixing time of 100 ms. For both the above experiments, the sample and acquisition conditions were the same as those for the ^1H−^{15}N HSQC experiment.

^{15}N-Labeled CaCeCb Sample. Two-dimensional (2D) ^1H−^{15}N HSQC experiments were performed after each addition

of GdmHCl at 16.4 T (700 MHz proton Larmor frequency). The acquisition conditions were the same as those for the measurements with the [^{15}N]Ca_2Cb sample.

^{15}N-Labeled Apo-Cb Sample. Two-dimensional (2D) ^{1}H−^{15}N HSQC experiments were performed after each addition of GdmHCl at 9.4 T (400 MHz proton Larmor frequency). The acquisition conditions were the same as those for the measurements with the [^{15}N]Ca_2Cb sample.

All NMR data were processed with the Bruker XWIN-NMR software package.

NMR Restraints

NOESY Restraints. The dipole−dipole restraints used in this work are those obtained from NOESY and 1D NOE experiments for Calbindin D_{9k} in which the native calcium in site II is replaced with cerium (CaCeCb hereafter), as previously reported (*3*).

Pseudocontact Shifts. Pseudocontact shifts (pcs) are introduced as constraints in the target function of PARAMAGNETIC-DYANA (*36*) calculations as a sum of differences between the experimental and the calculated pcs for the observed nuclei in each family of structures according to the previously reported procedure (*36*, *37*). The experimental pseudocontact shifts for ^{15}N and backbone ^{1}H atoms of the CaCeCb derivative in the presence of 2 M GdmHCl were obtained from the observed chemical shifts according to the expression

$$\delta^{\mathrm{exp}} = \delta^{\mathrm{dia}} + \delta^{\mathrm{pcs}}$$

where δ^{dia} is the chemical shift of the corresponding nucleus in the Ca_2Cb native protein in the presence of 2 M GdmHCl. The calculated δ^{pcs} values were obtained by assuming the metal center point dipole approximation, i.e., by applying eq 1 to the corresponding nuclei.

$$\delta_i^{\mathrm{pcs}} = \frac{1}{12\pi r_i^3}\left[\Delta\chi_{\mathrm{ax}}(3\cos^2\theta_i - 1) + \frac{3}{2}\Delta\chi_{\mathrm{rh}}\sin^2\theta_i\cos 2\phi_i\right] \quad (1)$$

where $\Delta\chi_{\mathrm{ax}}$ and $\Delta\chi_{\mathrm{rh}}$ are the axial and rhombic anisotropy parameters, respectively, of the magnetic susceptibility tensor of the metal, r_i is the distance between atom i and the metal ion, and θ_i and ϕ_i are the spherical polar angles of atom i with respect to the principal axes of the magnetic susceptibility tensor centered on the metal ion. The magnetic anisotropy components as well as the orientation of the tensor were obtained using the program FANTASIA (*38*).

Structure Calculation

The modified version of the program DYANA (*39*), called PARAMAGNETIC-DYANA (*36*), which permits the use of pcs as constraints, was used for the structure calculations. Torsion angle dynamics (TAD) combined with a simulated annealing algorithm was used to calculate a family of 200 structures starting from randomly generated conformers in 10 000 annealing steps. The quality of structures calculated by PARAMAGNETIC-DYANA can be assessed by a properly defined function (target function) proportional to the squared deviations of the calculated constraints from the experimental ones, plus the squared van der Waals contact violations. In DYANA (and in PARAMAGNETIC-DYANA as well), the target function TF has the role of a pesudopotential energy and is defined so that TF = 0 if and only if all experimental distance constraints and torsion angle constraints are fulfilled and all nonbonded atom pairs satisfy a check for the absence of steric overlap (*39*). TF values are expressed in square angstroms. Mean structures obtained were minimized using the program PARAMAGNETIC-DYANA with a 1000 steps conjugate gradient minimization.

The programs RASMOL and PROCHECK-NMR were subsequently used to analyze the calculated structures.

RESULTS

NMR Titration with GdmHCl. The changes in ^{1}H and ^{15}N shift values for the Ca_2Cb and CaCeCb derivatives were followed by titrating the protein with increasing amounts of GdmHCl and acquiring both 1D ^{1}H and 2D ^{1}H−^{15}N HSQC spectra after each addition of denaturant to the protein samples.

In the range of GdmHCl concentrations that was used (0−2 M), chemical shift differences for H_N in either Ca_2Cb or CaCeCb are small and close to zero; the pattern is the same in both proteins and reproducible. Larger chemical shift changes are observed in CaCeCb in the region of isotropically shifted signals. Overall, observed changes are up to 2 ppm for the hyperfine-shifted signals and up to 0.3 ppm for the diamagnetic signals.

Differences in chemical shifts of ^{15}N resonances are bigger, some of them more than 1 ppm. As previously reported (*40*, *41*), these differences are likely correlated to some charge-dependent mechanism. No concomitant decrease in intensity of any HSQC peak was observed. The very small chemical shift differences and the lack of intensity changes indicate that, at 2 M GdmHCl, the overall folding of CaCeCb is conserved, and that no exchange equilibrium is present between two or more species.

To acquire information about protein stability, we titrated the nonlabeled CaCeCb protein to a guanidinium chloride concentration of 5.5 M. No exchange phenomena and no loss of secondary structure were observed, in agreement with data reported in the literature, indicating that the metal-containing protein is very resistant to denaturation (*11*). This structural stability prevents us from performing a two-state model fitting (native-unfolded) (*42*) as used in previous works (*23*, *43*, *44*) to obtain the free energy of unfolding in the absence of denaturant ($\Delta G°$). On the contrary, when the titration was performed on the apo form of the protein, loss of secondary structure was observed for a denaturing concentration of 3.3 M, consistent with previous findings.

Fast Protein Dynamics via Cross Correlation Experiments. Fast protein dynamics are usually evaluated via the rather tedious and experimentally time-consuming so-called ModelFree approach (*45*−*47*). However, it has been pointed out by Bax *et al*. (*33*) that much simpler relaxation interference experiments between ^{15}N chemical shit anisotropy (CSA) and ^{1}H−^{15}N dipole−dipole coupling give equivalent information about the order parameters (S^2) with a precision of 5−10%. We have performed such cross correlation experiments on the Ca_2Cb sample at 2 M GdmHCl, and compared the results with those obtained at 0 M GdmHCl (*48*).

Measured cross correlation rates (ccr hereafter) range from 4.6 to 10.2 s^{-1} and from 4.6 to 13.4 s^{-1} at 0 and 2 M

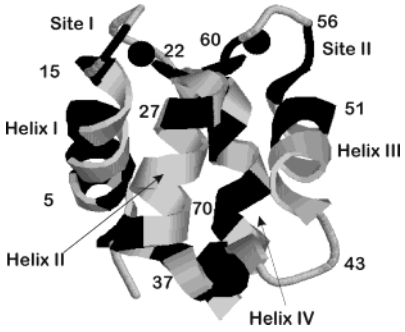

FIGURE 1: Schematic drawing of Ca_2Cb. Residues shown in dark gray correspond to those backbone atoms for which a decrease in cross correlation rates larger than 0.6 s^{-1} was measured when passing from 0 to 2 M GdmHCl.

GdmHCl, respectively (Supporting Information, Table S1). Although, on average, ^{15}N CSA and dipole−dipole ccr show an only 5% decrease on passing from 0 to 2 M GdmHCl, there are amino acids that experience a variation of up to 25%.

Residues whose cross correlation rates decrease by more than 0.6 s^{-1} on passing from 0 to 2 M GdmHCl are shown in dark gray in Figure 1. As found for the native state of the protein (*48*), rates smaller than the average are observed in the linker region and are indicative of fast internal dynamics. Under non-native conditions, the four helices show a much larger spreading and slightly smaller rates with respect to the native state. Within each EF-hand, the two helices exhibit a different behavior, helices I and IV being much more affected by the presence of GdmHCl than helices II and III. Also, the two metal binding domains do not behave in the same way. Indeed, the regular EF-hand loop (site II) appears to be much more affected by GdmHCl than the pseudo-EF-hand (site I).

The behavior of hydrophobic core residues is significant. The hydrophobic core is formed by packing of hydrophobic side chains belonging to the four helices as well as to the two binding loops. Structural studies point out that hydrophobic core is formed by the following residues: Leu6, Ile9, Phe10, Leu23, Leu28, Leu31, Leu32, Leu46, Leu49, Phe50, Leu53, Val61, Phe66, Leu69, Val70, and Ile73 (*7*). Some of the hydrophobic residues that belong to helix IV experience a substantial decrease in ccr with respect to that under native conditions. In sites I and II, residues Leu23 and Val61, which also belong to the hydrophobic core of the protein and are part of the antiparallel β-strand region forming a two-way interdomain H-bond, exhibit lower rates. This provides spectroscopic evidence that the H-bond between the two residues is broken, thus allowing less restricted internal motions for Leu23 and Val61.

Finally, there are residues that exhibit an increase in ccr upon addition of GdmHCl. In particular, residues Asp19, Glu27, Glu48, Ser62, and Val68 experience an increase in their rates of more than 0.7 s^{-1}.

Slow Protein Dynamics As Measured via T_2 CPMG Experiments. Protein motions on the microsecond to millisecond time scales are normally due to chemical or conformational kinetic phenomena (*49*, *50*). Such exchange processes contribute to the transverse relaxation rate and can be quantified by ^{15}N NMR relaxation measurements for the amide backbone resonances using CPMG (laboratory frame) T_2 experiments at variable τ_{cp} (*32*, *50*). ^{15}N $R_2(1/\tau_{cp})$ values

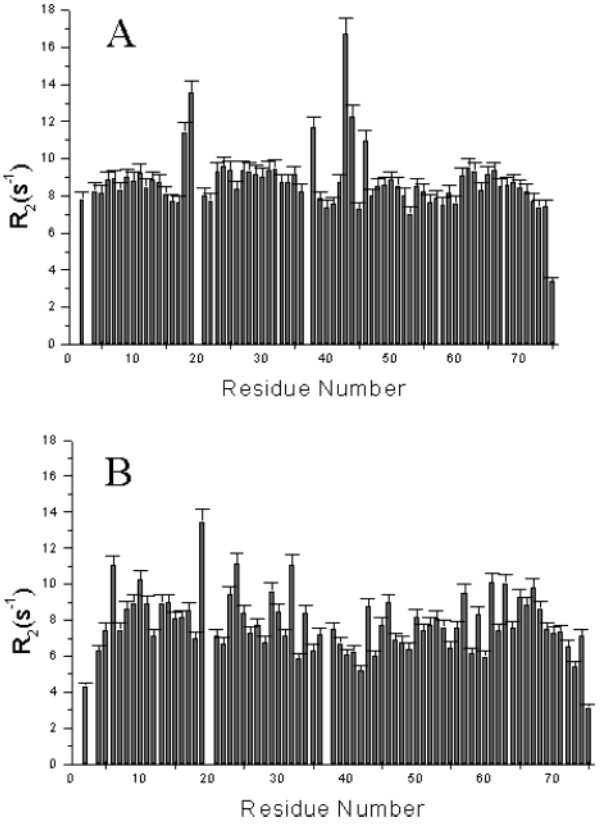

FIGURE 2: Comparison of R_2 values measured for Ca_2Cb at 0 (*48*) (A) and 2 M GdmHCl (B). Values were collected at 700 MHz, using the relaxation-compensated T_2 CPMG sequence (*32*) with a τ_{cp} of 1 ms.

were measured on the Ca_2Cb form of the protein in the presence of 2 M GdmHCl. A lack of observable dispersion was observed in plots of R_2 versus $1/\tau_{cp}$ over the experimentally accessible range in the protein (data not shown).

R_2 values obtained with a τ_{cp} of 1 ms can be compared with data previously collected on the native form of the protein (*48*). Two main features are observed as shown in Figure 2. (i) An exchange contribution to R_2, observed in the native form for residues 18, 38, 43, 44, and 46, is not present at 2 M GdmHCl. (ii) The behavior of R_2 values versus the amino acidic sequence is very similar to that observed for cross correlation rates. In particular, residues belonging to the hydrophobic core of the protein are almost unaffected by the presence of GdmHCl, while solvent-exposed ones experience increases in R_2 values.

Amide Proton Exchange Rates. Conformational exchange phenomena which open parts of the protein backbone and expose it to bulk solvent are expected to give rise to relatively fast amide proton exchange kinetics for the exposed residues. Amide proton exchange in the range from 0.1 to 90 s^{-1} is easily assessed via (CLEANEX-PM)−HSQC experiments (*34*, *35*). We have acquired the ^{15}N (CLEANEX-PM)−FSQC spectrum for the Ca_2Cb sample at 2 M GdmHCl. The spectrum is the same as that obtained without denaturant (*48*).

Pseudocontact Shifts. From the analysis of chemical shift values obtained for both Ca_2Cb and CaCeCb at 0 and 2 M GdmHCl, slight changes in pcs for both ^{15}N and H_N resonances have been observed. In particular, residues in sites I and II endure the largest changes, as shown in Figure 3. The general trend is the same at both concentrations of the

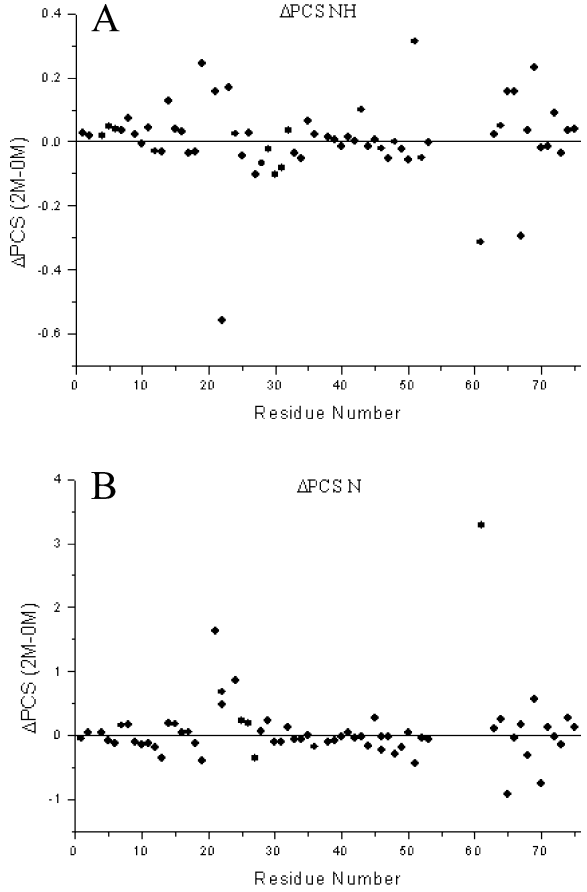

FIGURE 3: Observed differences between pseudocontact shifts measured at 2 and 0 M GdmHCl for the CaCeCb derivative. Values are reported for HN (A) and N (B) backbone resonances. All reported values are reported according to the equation $\Delta\delta = [\delta(\text{Ce,2 M}) - \delta(\text{Ca,2 M})] - [\delta(\text{Ce,0 M}) - \delta(\text{Ca,0 M})]$.

denaturant, but there are nine residues, namely, residues 19 and 21−24 (site I) and 61 and 64 (site II), which, together with residues 69 and 70, which belong to the C-terminus of the protein, present quite different values of pcs due to the presence of GdmHCl.

Pcs values obtained at 2 M GdmHCl are used to recalculate the orientation of the magnetic axes and the magnitude of the main components of the magnetic susceptibility tensor for the CaCeCb derivative by running the program FANTASIA (*38*). The values obtained in the present work are as follows: $\Delta\chi_{ax} = 2.20 \times 10^{-32}$ m^3 and $\Delta\chi_{rh} = 0.60 \times 10^{-32}$ m^3. They are very similar to those of the native state: $\Delta\chi_{ax} = 2.08 \times 10^{-32}$ m^3 and $\Delta\chi_{rh} = 0.71 \times 10^{-32}$ m^3 (*6*).

Solution Structure Calculations. Structure calculations were performed with the program PARAMAGNETIC-DYANA (*36*). The structure [PDB entry 1N65 (*51*)] consists of four helices and three loops, of which the first and third constitute the metal-binding site. Such an ensemble of conformers has a root-mean-square deviation (rmsd) for the backbone atoms of 0.71 ± 0.23 Å. The target function obtained for this family of structures ranges from 1.10 to 1.15 Å^2. Most of the contributions to target function arise from pcs constraints (87%), and no consistent violations between NOESY constraints were found.

Even if more than 1000 NOESY constraints from the native form of the protein were used, the obtained structure is different from that of the native state. The structure of the native protein, obtained with the same NOESY constraints and pcs values at 0 M GdmHCl, has a backbone rmsd of 0.67 ± 0.22, while the target function ranges from 0.64 to 0.71 Å^2. The rmsd for the backbone atoms of native and non-native states is 0.48 Å, and the rmsd (BB) plot per residue between the native and unfolded structure is given in Figure 4 (●). Secondary structure elements and the overall four-helix bundle fold are not affected by the mild denaturant concentration; nevertheless, both metal binding loops and the linker region do experience structural variations.

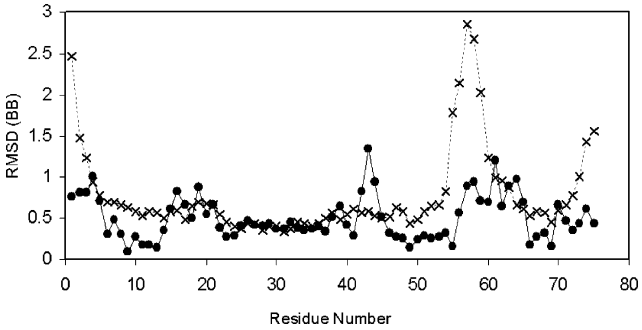

FIGURE 4: Pairwise rmsd (●) between the CaCeCb structure obtained at 0 M GdmHCl and the CaCeCb structure obtained at 2 M GdmHCl. The two structures were obtained using the same set of NOE values and a different set of pseudocontact shifts and magnetic anisotropy tensor. The sum of rmsd values obtained for the two structures is also shown (×). The latter is used as a threshold to monitor those regions in which observed structural differences are meaningful.

DISCUSSION

The body of the experimental NMR data acquired for the Ca_2Cb and CaCeCb derivatives under non-native conditions provides a complete picture of the structural and dynamical features of this system and may contribute to a more complete understanding of the folding properties of Calbindin D_{9k}. Extensive studies have been performed in the past on the WT protein and on various mutants in an effort to obtain information about its stability and function (*11*, *30*, *52*).

All the previous studies have shown that reduction of the stability of the hydrophobic core is not sufficient in itself to induce the opening of the protein core even under very strong denaturing conditions. Therefore, large alterations in stability seem to be tolerated by the protein while it retains its fold and conformational response to calcium binding. It has been shown that the CaCeCb protein is stable at high denaturant concentrations while Calbindin D_{9k} loses its structure at relatively low denaturant concentrations when no metal is coordinated. This permits us to state that not only Ca^{2+} but also Ce^{3+} contribute to the protein stability.

The analysis of fast protein dynamics at 0 and 2 M GdmHCl measured on the diamagnetic Ca_2Cb indicates that the outer residues of the helices do experience a reduction in the cross correlation rates while the hydrophobic part of the helices is almost unaltered. This supports the picture that hydrophobic interactions occurring between the helices are the driving force of the four-helix bundle fold. An interesting result is the increase in ccr rates for residues 19, 27, 43, 48, 62, and 68. All of them, with the notable exception of residue 19, whose backbone carbonyl is coordinating the calcium ion, are close in sequence to residues belonging to the hydrophobic core of the protein. Their non-negligible

increased rigidity at 2 M GdmHCl can be therefore related to a closer and stronger packing of the hydrophobic interactions in the protein as a response to the presence of denaturing agents in solution.

The different topology between EF-hand and pseudo-EF-hand loops provides them with different properties. This was previously pointed out by dynamics and mutagenesis studies (*11*, *30*, *52*), and it is remarkable that under non-native conditions this feature becomes more evident. At 2 M GdmHCl, site I retains in an unaltered form the dynamic properties of the native state, with the exception of residue 19 that experiences an increased rigidity. This suggests that backbone dynamics are essentially driven by the binding of the metal ion and that mild concentrations of the denaturant have only small effects on the affinity of pseudo-EF-hand versus Ca^{2+}. On the other hand, site II experiences a more generalized decrease in ccr rates. Indeed, when the metal coordination is mostly provided by carboxylate groups of side chains such as in the classical EF-hand site II of Cb, the backbone dynamics of the metal binding loop are expected to be less hindered by the metal ion, much less dependent on the chromophore, and therefore much more dependent on the solution environment.

The behavior of hydrophobic residues is also interesting. Indeed, not all the hydrophobic core residues are equally affected by the addition of denaturing agents. While for residues belonging to helices I−III the observed differences in cross correlation rates between 0 and 2 M GdmHCl are, on average, zero, the hydrophobic residues of helix IV, namely, residues 66, 69, 70, and 73, do experience lower rates at 2 M GdmHCl. Previously observed differences between the structures of apo Cb and Ca_2Cb in helix IV have been associated with a subtle reorganization of the hydrophobic core (*53*). These data agree with our findings and point out that the hydrophobic core region around helix IV constitutes a sort of weak part in the hydrophobic core of the protein.

The observed decrease in cross correlation rates of the two residues involved in a two-way long-range H-bond (namely, residues 23 and 61) suggests that, even at low concentrations of GdmHCl, there can be subtle structural variations in the relative position of the two protein subdomains. The increased dynamics of Leu23 and Val61 are likely to cause the disruption of such an H-bond bridge which, in turn, has an important role in the relative position of the two EF-hand domains. Such changes in cross correlation rates may be precipitated by structural effects, as shown by the comparison of structures in solution in native and non-native states.

T_2 CPMG experiments further contribute to the understanding of the behavior of the system under non-native conditions. On one hand, the absence of any dependence of T_2 values on the τ_{cp} delay is consistent with the results obtained for Ca_2Cb in the native form (*48*). On the other hand, T_2 values collected using a τ_{cp} of 1 ms at 0 and 2 M GdmHCl indicate that the exchange contribution (millisecond dynamics) observed in the native protein for some residues of the hydrophobic pocket is not present at 2 M GdmHCl. In particular, only residue 19 retains the exchange contribution to T_2^{-1} found for the native form of the protein. Slow dynamics observed in the native state have been related to a redirection of the Met43 side chain to the protein core inducing conformational exchange in residues belonging to the hydrophobic core of the protein (*48*). Mild charged denaturing agents are likely to freeze the conformational exchange of the Met43 hydrophobic side chain as well as that of residues 18, 38, 44, and 46, which are involved in this rearrangement. This is in perfect agreement with the fast protein dynamics findings, since ccr values indicate that Met43 has a more restricted motion at 2 M GdmHCl, suggesting a complete redirection of its side chain toward the protein core.

To address structural changes at 2 M GdmHCl, we focused on the information arising from the hyperfine interaction. The availability of pcs data makes it possible to recalculate the structure simply using the NOEs collected on the native state of the protein together with pcs data collected at 2 M GdmHCl. The absence of consistent violations between NOESY constraints as well as the rmsd observed between the two structures (native and non-native) indicates that early steps of the unfolding produce small structural rearrangements that do not affect the NOESY constraints, probably because they are within the tolerance of these constraints. Still, such rearrangements can be monitored by pcs constraints, and the observed structural differences between the native form and the 2 M GdmHCl state can be safely analyzed. The same approach has recently been used to monitor temperature-dependent structural changes. Different sets of pcs collected at different temperatures in the range of 280−310 K were used together with a single set of NOE data, collected at 300 K, to monitor temperature-dependent structural changes (*54*).

Figure 4 reports the rmsd per residue observed between the structure recalculated at 2 M GdmHCl and the structure of the native form. The overall rmsd between the native and non-native state (0.48 Å) is much smaller than those observed in other early steps of unfolding processes. The rmsd values below 1.0 Å are also observed among structures of the same protein obtained with a different set of constraints (e.g., without pcs, rdc, or both) (*44*). The rmsd values around 0.3 Å are usually observed between different X-ray structures of the same protein obtained in different crystal forms (*55*). Therefore, the observed rmsd value is indicative of very subtle structural changes and is somewhat at the borderline of significance. Still, the observed differences are localized well and therefore point out those protein regions that undergo structural rearrangements upon interaction with GdmHCl. There are three regions where the rmsd between the two average structures is significantly larger than the sum of the rmsd values of the two families, which is also shown in Figure 4 and which can be safely considered the threshold for discrimination of structural changes. Three residues for each of the metal binding sites and for the linker region are, together with residue 39, which is also close to the linker region, above the sum of the rmsd values of the two families. This indicates that the two domains undergo some change in their relative orientation. In the family of structures obtained under non-native conditions, only three of 20 conformers retain the two-way H-bond between Leu23 and Val61. The observed structural change of this H-bond, which in the native state forms the only interdomain contact in the entire protein, supports the rearrangement supposed from the fast dynamics results. This rearrangement may also affect the overall shape of the protein as can be observed from the small change in the magnetic anisotropy tensor obtained from

pcs values. Consistent with the different topology of the two metal binding domains, site II, which binds the metal via side chains, exhibits on average larger structural rearrangements than the more rigid site I. It is the linker region, and in particular residue Met43, that undergoes the larger structural changes when passing from the native state to 2 M GdmHCl. As suggested by the analysis of dynamics data, this can be explained by supposing a complete reorientation of the hydrophobic Met43 side chain toward the protein core to minimize the interaction with the charged denaturing agent present in solution.

Given the high stability of both Ca_2Cb and CaCeCb, a GdmHCl concentration of 2 M is not sufficient to change the overall fold of the system. Since only very small chemical shift differences and no intensity change in $^1H-^{15}N$ HSQC peaks were observed, no exchange phenomena are present between two or more forms of the protein. The protein is basically in a near-native state very close in energy, structure, and mobility to the native one. In terms of energy landscape (*25*, *56*), the near-native state at 2 M GdmHCl corresponds to a conformation that differs from the native one for the fraction of native contacts (Q_0), and therefore for the total free energy. This conformation is found near the bottom of the "funnel-like" shape that defines the accessible free energy surface of the protein, but does not correspond to the unique (lowest-energy) native conformation. These results are similar to those obtained for cytochrome b_5 in the presence of a low GdmHCl concentration (*23*).

Concluding Remarks. Even when kinetic aspects of folding and unfolding processes are neglected, it is very difficult not only to characterize but also to identify the occurrence of structural and/or dynamics perturbations arising from the presence of non-native conditions. For several years, NMR spectroscopy has been considered the best technique for monitoring the occurrence of those non-native states (*19*, *57*−*59*), yet how sensitive NMR can be is, of course, a difficult question to address.

In the case of Calbindin D_{9k}, our results point out that, even at a mild concentration of a denaturing agent (2 M GdmHCl) and although no major changes occur in terms of the overall molecular fold, there are several events that can be monitored. Hydrophobic and hydrophilic residues of the four-helix bundle domain undergo different changes in local dynamics, showing a somehow tighter packing of the hydrophobic core of the protein. Within the hydrophobic core, residues belonging to helix IV are much more affected than residues arising from helices I−III by changes in the solution environment. A complete reorientation of the Met43 side chain toward the hydrophobic core is accomplished by the disappearance of the millisecond dynamics observed on the native form of Calbindin. The two metal binding domains have a different behavior under mild denaturing conditions, consistent with their topology. The addition of 2 M GdmHCl to Ca_2Cb and CeCaCb gives access to a near-native state of the protein. Both the structure and dynamics of the this near-native state can be characterized with the same precision of the native state. The exploitation of long-range paramagnetism-based constraints available for the CaCeCb derivative allows us to monitor the subtle structural changes in the interdomain orientation occurring in Calbindin D_{9k} at 2 M GdmHCl without any need for additional NOESY experiments and assignments. Information derived from the analysis of pseudocontact shifts allows us to monitor the small variation in the magnetic anisotropy tensor and to recalculate a structure in solution that allows a fine mapping of structural events under non-native conditions.

In conclusion, it is well established that paramagnetic probes provide precious structural information. The results presented here point out that another feature of paramagnetism-based constraints is sensitivity. This, in our opinion, is going to be extremely useful and widely exploited in the next future. Whenever applicable, this approach promises to be a key to improving the ability of NMR spectroscopy to address small fluctuation and local conformational changes.

ACKNOWLEDGMENT

We are grateful to Prof. Ivano Bertini and Prof. Claudio Luchinat for their advice and discussions.

SUPPORTING INFORMATION AVAILABLE

Cross correlation rates measured for Ca_2Cb at 0 and 2 M GdmHCl. This material is available free of charge via the Internet at http://pubs.acs.org.

REFERENCES

1. Heizmann, C. W., and Hunziker, W. (1991) *Trends Biochem. Sci. 16*, 98−103.
2. Kretsinger, R. H., and Nockolds, C. E. (1973) *J. Biol. Chem. 248*, 3313−3326.
3. Allegrozzi, M., Bertini, I., Janik, M. B. L., Lee, Y.-M., Liu, G., and Luchinat, C. (2000) *J. Am. Chem. Soc. 122*, 4154−4161.
4. Banci, L., Bertini, I., and Luchinat, C. (1985) in *Rare Earths Spectroscopy* (Trebiatowska, B. J., Legendziewicz, J., and Strek, W., Eds.) pp 80−99, World Scientific, Singapore.
5. Bentrop, D., Bertini, I., Cremonini, M. A., Forsén, S., Luchinat, C., and Malmendal, A. (1997) *Biochemistry 36*, 11605−11618.
6. Bertini, I., Janik, M. B. L., Lee, Y.-M., Luchinat, C., and Rosato, A. (2001) *J. Am. Chem. Soc. 123*, 4181−4188.
7. Svensson, L. A., Thulin, E., and Forsén, S. (1992) *J. Mol. Biol. 223*, 601−606.
8. Kordel, J., Skelton, N. J., and Chazin, W. J. (1993) *J. Mol. Biol. 231*, 711−734.
9. Bertini, I., Donaire, A., Jimenez, B., Luchinat, C., Parigi, G., Piccioli, M., and Poggi, L. (2001) *J. Biomol. NMR 21*, 85−98.
10. Bertini, I., Lee, Y.-M., Luchinat, C., Piccioli, M., and Poggi, L. (2001) *ChemBioChem 2*, 550−558.
11. Julenius, K., Thulin, E., Linse, S., and Finn, B. E. (1998) *Biochemistry 37*, 8915−8925.
12. Akke, M., and Forsén, S. (1990) *Proteins: Struct., Funct., Genet. 8*, 23−29.
13. Wendt, B., Hofmann, T., Martin, S. R., Bayley, P. M., Brodin, P., Grundstrom, T., Thulin, E., Linse, S., and Forsén, S. (1988) *Eur. J. Biochem. 175*, 439−445.
14. Finn, B. E., Kordel, J., Thulin, E., Sellers, P., and Forsén, S. (1992) *FEBS Lett. 298*, 211−214.
15. Dill, K. A., and Shortle, D. (1991) *Annu. Rev. Biochem. 60*, 795−825.
16. Shortle, D. (1996) *Curr. Opin. Struct. Biol. 6*, 24−30.
17. Smith, L. J., Bolin, K. A., Schwalbe, H., MacArthur, M. W., Thornton, J. M., and Dobson, C. M. (1998) *Folding Des. 1*, R95−R106.
18. Neri, D., Billeter, M., Wider, G., and Wüthrich, K. (1992) *Science 257*, 1559−1563.
19. Buck, M., Schwalbe, H., and Dobson, C. M. (1995) *Biochemistry 34*, 13219−13232.
20. Logan, T. M., Theriault, Y., and Fesik, S. W. (1994) *J. Mol. Biol. 236*, 637−648.
21. Farrow, N. A., Zhang, O., Forman-Kay, J. D., and Kay, L. E. (1997) *Biochemistry 36*, 2390−2402.
22. Zhang, O., Kay, L. E., Shortle, D., and Forman-Kay, J. D. (1997) *J. Mol. Biol. 272*, 9−20.
23. Arnesano, F., Banci, L., Bertini, I., and Koulougliotis, D. (1998) *Biochemistry 37*, 17082−17092.

24. Bentrop, D., Bertini, I., Iacoviello, R., Luchinat, C., Niikura, Y., Piccioli, M., Presenti, C., and Rosato, A. (1999) *Biochemistry 38*, 4669−4680.
25. Dobson, C. M., and Karplus, M. (1999) *Curr. Opin. Struct. Biol. 9*, 92−101.
26. Schwalbe, H., Grimshaw, S. B., Spencer, A., Buck, M., Boyd, J., Dobson, C. M., Redfield, C., and Smith, L. J. (2001) *Protein Sci. 10*, 677−688.
27. Wain, R., Pertinhez, T. A., Tomlinson, E. J., Hong, L., Dobson, C. M., Ferguson, S. J., and Smith, L. J. (2001) *J. Biol. Chem. 276*, 45813−45817.
28. Brodin, P., Grundstrom, T., Hofmann, T., Drakenberg, T., Thulin, E., and Forsén, S. (1986) *Biochemistry 25*, 5371−5377.
29. Johansson, C., Brodin, P., Grundstrom, T., Thulin, E., Forsén, S., and Drakenberg, T. (1990) *Eur. J. Biochem. 187*, 455−460.
30. Malmendal, A., Carlström, G., Hambraeus, C., Drakenberg, T., Forsén, S., and Akke, M. (1998) *Biochemistry 37*, 2586−2595.
31. Chazin, W. J., Kördel, J., Drakenberg, T., Thulin, E., Brodin, P., Grundstrom, T., and Forsén, S. (1989) *Proc. Natl. Acad. Sci. U.S.A. 86*, 2195−2198.
32. Millet, O., Loria, J. P., Kroenke, C. D., Pons, M., and Palmer, A. G., III (2000) *J. Am. Chem. Soc. 122*, 2867−2877.
33. Tjandra, N., Szabo, A., and Bax, A. (1996) *J. Am. Chem. Soc. 118*, 6986−6991.
34. Hwang, T. L., Mori, S., Shaka, A. J., and Van Zijl, P. C. M. (1997) *J. Am. Chem. Soc. 119*, 6203−6204.
35. Hwang, T. L., Van Zijl, P. C. M., and Mori, S. (1998) *J. Biomol. NMR 11*, 221−226.
36. Barbieri, R., Bertini, I., Cavallaro, G., Lee, Y. M., Luchinat, C., and Rosato, A. (2002) *J. Am. Chem. Soc. 124*, 5581−5587.
37. Banci, L., Bertini, I., Cremonini, M. A., Gori Savellini, G., Luchinat, C., Wüthrich, K., and Güntert, P. (1998) *J. Biomol. NMR 12*, 553−557.
38. Banci, L., Bertini, I., Gori Savellini, G., Romagnoli, A., Turano, P., Cremonini, M. A., Luchinat, C., and Gray, H. B. (1997) *Proteins: Struct., Funct., Genet. 29*, 68−76.
39. Güntert, P., Mumenthaler, C., and Wüthrich, K. (1997) *J. Mol. Biol. 273*, 283−298.
40. Bertini, I., Luchinat, C., and Turano, P. (2000) *J. Biol. Inorg. Chem. 5*, 761−764.
41. Boyd, J., Dobson, C. M., Morar, A. S., Williams, R. J. P., and Pielak, G. J. (1999) *J. Am. Chem. Soc. 121*, 9247−9248.
42. Santoro, M. M., and Bolen, D. W. (1988) *Biochemistry 27*, 8063−8068.
43. Bertini, I., Cowan, J. A., Luchinat, C., Natarajan, K., and Piccioli, M. (1997) *Biochemistry 36*, 9332−9339.
44. Arnesano, F., Banci, L., Bertini, I., Koulougliotis, D., and Monti, A. (2000) *Biochemistry 39*, 7117−7130.
45. Halle, B., and Wennerström, H. (1981) *J. Chem. Phys. 75*, 1928−1943.
46. Lipari, G., and Szabo, A. (1982) *J. Am. Chem. Soc. 104*, 4559−4570.
47. Lipari, G., and Szabo, A. (1982) *J. Am. Chem. Soc. 104*, 4546−4559.
48. Bertini, I., Carrano, C. J., Luchinat, C., Piccioli, M., and Poggi, L. (2002) *Biochemistry 41*, 5104−5111.
49. Kay, L. E. (1998) *Nat. Struct. Biol. 5*, 513−517.
50. Ishima, R., and Torchia, D. A. (2000) *Nat. Struct. Biol. 7*, 740−743.
51. Berman, H. M., Westbrook, J., Feng, Z., Gilliland, G., Bhat, T. N., Weissig, H., Shindyalov, I. N., and Bourne, P. E. (2000) *Nucleic Acids Res. 28*, 235−242.
52. Kragelund, B. B., Jönsson, M., Bifulco, G., Chazin, W. J., Nilsson, A., Finn, B. E., and Linse, S. (1998) *Biochemistry 37*, 8926−8937.
53. Skelton, N. J., Kordel, J., and Chazin, W. J. (1995) *J. Mol. Biol. 249*, 441−462.
54. Allegrozzi, M., Bertini, I., Choi, S. N., Lee, Y.-M., and Luchinat, C. (2002) *Eur. J. Inorg. Chem.*, 2121−2127.
55. Gallagher, T., Alexander, P., and Gilliland, G. L. (1994) *Biochemistry 33*, 4721−4729.
56. Dobson, C. M., Sali, A., and Karplus, M. (1998) *Angew. Chem., Int. Ed. 37*, 868−893.
57. Balbach, J., Forge, V., Van Nuland, N. A. J., Winder, S. L., Hore, P. J., and Dobson, C. M. (1995) *Nat. Struct. Biol. 2*, 865−870.
58. Miranker, A., Radford, S. E., Karplus, M., and Dobson, C. M. (1991) *Nature 349*, 633−635.
59. Wain, R., Pertinhez, T. A., Tomlinson, E. J., Hong, L., Dobson, C. M., Ferguson, S. J., and Smith, L. J. (2001) *J. Biol. Chem. 276*, 45813−45817.

BI034638+